Big Data and Information Analytics

https://www.aimspress.com/journal/BDIA

BDIA, 8: 1–25.
DOI:10.3934/bdia.2024001
Received: 29 May 2024
Revised: 18 June 2024
Accepted: 20 June 2024
Published: 03 July 2024

Research article

Dynamic mode decomposition for blindly separating mixed signals and decrypting encrypted images

Cun Chen[1,*] **and Hui Peng**[2]

[1] School of Mathematics and Statistics, Zhengzhou University, Zhengzhou 450001, China

[2] Data Center of Science and Technology Information, Wuhan Marine Machinery Plant Co., LTD., Wuhan 430084, China

* **Correspondence:** Email: chencun@zzu.edu.cn.

Abstract: In this paper, we introduce the dynamic mode decomposition considering a lag τ (τ-DMD) for solving the blind source separation (BSS) problem of chaotic signals and images. τ-DMD can be used in BSS-based image decryption with good separation performance. The unmixing problem was formulated as a modal decomposition problem. τ-DMD was applied on separating linear mixed chaotic signals showing a better separation performance than the existing blind source separation algorithms (Amuse, SOBI, FastICA and JADE). In addition, the case of adding noise in the mixing process was considered, and wavelet de-nosing before τ-DMD improved the separation performance. For the application, τ-DMD can be used to remove the noise in electrocardiograms (ECG) and the ocular artifacts in electroencephalograms (EEG). τ-DMD can also be applied in image processing, showing good separation performance of τ-DMD for both synthetic mixtures and real-life mixed texts. Structural similarity index measurement (SSIM) and peak signal-to-noise ratio (PSNR) were selected as the evaluation criteria. We tested the separation performance of τ-DMD on natural images, fingerprint images, and real-life text images and compared the results with other methods. Furthermore, τ-DMD was applied to decrypt the BSS-based encrypted images. In the process of encryption, we set up the underdetermined problem of BSS by mixing the original and key images, and then τ-DMD was used to extract the original images in the process of decryption with the secret seeds provided. Two simulations were performed to illustrate the performance of τ-DMD for image decryption, showing a better decryption results than FastICA.

Keywords: dynamic mode decomposition; blind source separation; chaotic signal separation; image signal separation; images encryption and decryption

1. Introduction

Dynamic mode decomposition (DMD) originated from Koopman's work on nonlinear dynamical systems in 1931 [1]. Schmid and Sesterhenn defined the DMD algorithm for the first time and introduced it to fluid dynamics [2]. Rowley et al. [3] extended the DMD algorithm to nonlinear dynamics using the Koopman operator and demonstrated that under certain conditions, the DMD method can be viewed as the approximation of the infinite-dimensional Koopman operator by computing the eigenvalues and eigenvectors (low-dimensional modes) of a finite-dimensional linear model.

The DMD method decomposes a complex system into a set of non-orthogonal modes, which is used to demonstrate how the system evolves through snapshots or measurements in time. The goal of DMD is to find the best-fit linear operator A and its eigendecomposition. The decomposed eigenvectors correspond to the spatial modes (DMD modes), for each has a simple temporal behavior, while the corresponding eigenvalues define the growth/delay rates and oscillation frequencies. DMD is a regression algorithm that can be considered as a combination of principal component analysis (PCA) [4] and Fourier transforms [5]. Singular value decomposition (SVD) is the underlying algorithm of PCA, and it can provide effective dimensionality reduction in high-dimensional systems. However, SVD only provides modes that are entirely based on spatial correlation, while largely ignoring the temporal information. Each mode calculated by DMD consists of spatially correlated structures that have the same linear behavior in time [6]. Thus, DMD provides the information of how these dimensional reduced modes evolve in time, which is superior to SVD.

The blind source separation (BSS) originates from the problem of cocktail party [7], and the established theory of BSS has been widely used in speech signal processing and biomedicine [8, 9]. In general, the goal of BSS problem is to recover the source signals from the observed signals without any prior knowledge of the mixed channels and original sources. Methods based on second-order statistics or higher-order statistics to solve the BSS problem are shown in [10–13].

In our two versions of the BSS problem, source signals are generated by chaotic processes and images. Chaotic signals are nonlinear non-Gaussian signals, with the intrinsic characteristic of aperiodicity, sensitivity to initial values, and unpredictability, which makes it very difficult to recover from the mixed signals. For the mixed images, most of the important features (such as the edge feature and texture feature) in the image are included in the higher-order statistics of the image pixels. Blind separation of mixed images is also a difficult task, because source images are not independent of each other in most cases.

So far, no study has been reported on separating the above two types of signals by using DMD. Different from previous BSS methods, which are based on statistical information, we introduce the idea of DMD (decomposing a system into spatiotemporal coherent modes) to the BSS problem. In this paper, applying τ-DMD, we separate the linear mixtures of signals generated by chaotic systems. Moreover, it can accurately separate linear mixed images. Four test cases are used, including (i) a set of two different natural photographs, (ii) a set of two similar fingerprint images, (iii) a set of two different text images, and (iv) images decryption.

The main contributions of this work are as follows:

- We extend DMD (which is usually used for high-dimensional matrix) to low-dimensional signal matrix by using τ-DMD algorithm.

- We introduce the approach τ-DMD that relies only on data to solve the blind image separation problem and the blind chaotic signal separation problem.
- τ-DMD is introduced to separate mixed chaotic signals and mixed images for the first time, especially in images decryption. It shows better separation performance than other blind separation methods.

The following paragraphs of this paper are organized as follows: Section 2 reviews some related works. In Section 3, we introduce the methods in detail, including the BSS model, DMD algorithm, and τ-DMD algorithm. The simulation results are presented in Section 4, and the conclusion comes in Section V.

2. Materials and methods

2.1. DMD algorithm

DMD has been widely applied in diverse fields such as epidemiology, neuroscience, robotics, video processing, financial trading, and power systems [14–19]. Meanwhile, there have been some improvements based on the standard DMD algorithm. In [20], Kutz et al. combined the DMD method with multi-resolution analysis, resulting in a decomposition method that can separate complex systems into multi-resolution time-scale components. Chen et al. developed a method to improve the robustness of DMD to noise [5]. Recently, Brunton et al. extended DMD to the system with actuation and a large number of sub-sampling measurements [21]. Prasadan et al. applied the improved DMD method to the separation of time series [22].

2.2. Blind chaotic signal separation and blind image separation

In previous works, several algorithms have been proposed for BSS of chaotic signals. The separation of chaotic signals in [23] was carried out based on chaos synchronization. In [24], Feng et al. discussed the case of continuous-time chaotic source signals and proposed a fast random search (FRS) algorithm. Lo et al. [25] reduced the separation problem into an eigen problem considering different embedding spaces of chaotic signals. The blind separation of chaotic signals based on ICA is reported in [26]. The gradient method based on a proliferation exponent was used to separate the chaotic sources [27]. In a recent work [28], Sanjukta et al. utilized a technique called reservoir computing to separate the superimposed chaotic signals, which is a data-based separation method without knowledge of the dynamical equations.

Meanwhile, a number of methods have been proposed for blind image separation. For linear mixed images, Guidara et al. proposed a BSS method based on maximum likelihood [29]. Ning et al. used kurtosis maximization algorithm to realize the separation of instantaneous mixtures of images [30]. Hara et al. proposed a non-iterative method to separate linear mixed images using the boundary values of the determinant of the relative transformation matrix between the mixtures [31]. Abolghasemi used dictionary learning to solve image separation when the underlying sparse domain of the sources is not available [32]. Guo et al. applied entropy minimization for the solution of blind source separation problems in image analysis [33].

3. BSS model and DMD algorithm

3.1. The BSS model

The following is the BSS model of instantaneous linear mixing,

$$\boldsymbol{X}(t) = Q\boldsymbol{S}(t) + \boldsymbol{n}(t), (t = 1, 2, \cdots, N), \tag{3.1}$$

where $\boldsymbol{S}(t) = [S_1(t); S_2(t); \cdots; S_n(t)], (t = 1, 2, \cdots, N)$ is an n-dimensional matrix of unknown source signals; $\boldsymbol{X}(t) = [X_1(t); X_2(t); \cdots; X_m(t)], (t = 1, 2, \cdots, N)$ is the m-dimensional matrix of mixed signals; Q is an $m \times n$ mixed matrix of full column rank; $\boldsymbol{n}(t), (t = 1, 2, \cdots, N)$ is an m-dimensional additive Gaussian white noise with zero mean and σ^2 variance. Without consideration of noise, Eq (3.1) can be rewritten as

$$\boldsymbol{X}(t) = Q\boldsymbol{S}(t), (t = 1, 2, \cdots, N). \tag{3.2}$$

In the remaining part, we make the following underlying assumptions about the source signals in the BSS problem:

Assumption 1: The number of sources is required to be no larger than the number of measurements, i.e., $n \leq m$.

Assumption 2: The source components must have non-Gaussian distribution, or just one Gaussian signal at most.

Assumption 3: Rank(Q) = n.

Assumption 4: The components of the source matrix $\boldsymbol{S}(t)$ are $r - lag$ uncorrelated, i.e., the $r - lag$ covariance matrix $R_s(\tau) = E\{\boldsymbol{S}(t)\boldsymbol{S}^T(t+\tau)\}$ is diagonal.

Assumption 5: Source signal $\boldsymbol{S}(t)$ and noise $\boldsymbol{n}(t)$ are statistically independent, and $\boldsymbol{n}(t)$ is Gaussian noise with zero mean and $R_n(\tau) = E\{\boldsymbol{n}(t)\boldsymbol{n}^T(t+\tau)\} = \begin{cases} 0, \tau \neq 0; \\ \sigma^2 \mathrm{I}_m, \tau = 0; \end{cases}$.

The goal of the BSS is to find the demixing matrix W, recovering the source signals only according to the observed signals $\boldsymbol{X}(t), (t = 1, 2, \cdots, N)$, i.e.,

$$\boldsymbol{Y}(t) = W\boldsymbol{X}(t) = WQ\boldsymbol{S}(t) = PD\boldsymbol{S}(t), (t = 1, 2, \cdots, N), \tag{3.3}$$

where P is a permutation matrix that reflects the uncertainty of the order for the mixed matrix columns. D is a non-singular diagonal matrix with non-zero diagonal elements that reflects the uncertainty of the amplitude for the separated signals.

3.2. Standard DMD and τ-DMD

Consider the continuous nonlinear dynamic system

$$\frac{d\boldsymbol{x}}{dt} = f(\boldsymbol{x}, t; \mu), \tag{3.4}$$

where $\boldsymbol{x} \in \Re^n$ is a typically quite large vector $(n >> 1)$ representing the state of a dynamical system at time t, and μ is a set of parameters. Since the solution of Eq (3.4) is usually impossible to construct, we use numerical solutions to simulate the process. Given a set of the system state variables, $\boldsymbol{x}_k, (k = 1, 2, \cdots, N)$, where N is the total number of samples. Equation (3.4) is discretized into the form,

$$\boldsymbol{x}_{k+1} = F(\boldsymbol{x}_k), \tag{3.5}$$

by sampling at the time interval Δt, where $\boldsymbol{x}_k = \boldsymbol{x}(k\Delta t)$. The measures of the system state variables are denoted as $\boldsymbol{y}_k, (k = 1, 2, \cdots, N)$. The relationship between $\boldsymbol{x}_k$ and $\boldsymbol{y}_k$ is as follows,

$$\boldsymbol{y}_k = g(\boldsymbol{x}_k), \tag{3.6}$$

where $g()$ is a set of scalar-valued functions:

$$g : \mathscr{M} \to \mathscr{R}$$

$$\boldsymbol{x}_k \to g(\boldsymbol{x}_k). \tag{3.7}$$

By using Koopman operator κ, the analysis of finite-dimensional nonlinear dynamical systems can be transformed into that of infinite-dimensional linear systems, i.e., the Koopman operator κ acts on this set of observations:

$$\kappa g(\boldsymbol{x}_k) = g(F(\boldsymbol{x}_k)). \tag{3.8}$$

In many cases, the measures $\boldsymbol{y}_k$ are the state variables $\boldsymbol{x}_k$, i.e., $\boldsymbol{y}_k = g(\boldsymbol{x}_k) = \boldsymbol{x}_k$. The uniqueness of the DMD algorithm is an approximate estimate of the Koopman operator κ. More specifically, we obtain the local linear approximation of Eq (3.8) when we use a matrix A to approximate Koopman operator κ. Acorrding to Eqs (3.5) and (3.8), as well as $\kappa = A, g(\boldsymbol{x}_k) = \boldsymbol{x}_k$, it can be deduced that

$$\boldsymbol{x}_{k+1} = A\boldsymbol{x}_k. \tag{3.9}$$

The key idea of DMD algorithm is to use the matrices constructed by the state variables $\boldsymbol{x}_k (k = 1, 2, \cdots, N)$ to find the optimal A s.t. $\|\boldsymbol{x}_{k+1} - A\boldsymbol{x}_k\|_F$ is minimized for all $\boldsymbol{x}_k (k = 1, 2, \cdots, N-1)$. Arrange the N snapshots into two tall and skinny data matrices:

$$X = \begin{bmatrix} | & | & & | \\ \boldsymbol{x}_1 & \boldsymbol{x}_2 & \cdots & \boldsymbol{x}_{N-1} \\ | & | & & | \end{bmatrix}, \tag{3.10}$$

$$\begin{aligned} X' &= \begin{bmatrix} | & | & & | \\ \boldsymbol{x}_2 & \boldsymbol{x}_3 & \cdots & \boldsymbol{x}_N \\ | & | & & | \end{bmatrix} \\ &= \begin{bmatrix} | & | & & | \\ A\boldsymbol{x}_1 & A\boldsymbol{x}_2 & \cdots & A\boldsymbol{x}_{N-1} \\ | & | & & | \end{bmatrix}. \end{aligned} \tag{3.11}$$

These matrices can be written in the form

$$X' = AX. \tag{3.12}$$

The best-fit matrix A is given by

$$A = X'X^{\dagger}, \tag{3.13}$$

where † is the Moore-Penrose pseudoinverse. Note that the matrix A may be high dimensional, which makes it impossible to compute directly. However, the rank of A is at most N-1, which is much

smaller than $n(n >> 1)$. DMD circumvents the eigendecomposition of A by considering a rank-reduced representation in terms of a POD-projected matrix $\tilde{A}$. Figure 1 illustrates the idea of this strategy.

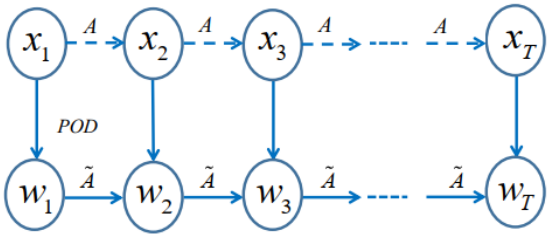

Figure 1. The schematic of the dimensional reduction process in DMD.

The DMD algorithm is as follows [34],

(1) Take the singular value decomposition (SVD) of X,

$$\begin{aligned} X &= U\sum V^* \\ &= \begin{bmatrix} \tilde{U} & \tilde{U}_{rem} \end{bmatrix} \begin{pmatrix} \tilde{\Sigma} & 0 \\ 0 & \Sigma_{rem} \end{pmatrix} \begin{bmatrix} \tilde{V}^* \\ \tilde{V}^*_{rem} \end{bmatrix}, \end{aligned} \tag{3.14}$$

where $*$ denotes the conjugate transpose, $\tilde{U} \in C^{n\times r}$,$\tilde{\Sigma} \in C^{r\times r}$, and $\tilde{V} \in C^{m\times r}$. r indicates the truncated rank and the index *rem* indicates the remaining $(N-1)-r$ singular values. The reason why we use truncation here is that it usually takes only a limited number of singular values connected with the dominant modes. So we can get the following approximation of X,

$$X = \tilde{U}\tilde{\Sigma}\tilde{V}^*. \tag{3.15}$$

(2) The matrix A can be obtained by Eqs (3.13) and (3.15),

$$A = X'\tilde{V}\tilde{\Sigma}^{-1}\tilde{U}^*. \tag{3.16}$$

using the $r \times r$ POD projection, we can get the low rank matrix

$$\tilde{A} = \tilde{U}^* A\tilde{U} = \tilde{U}^* X'\tilde{V}\tilde{\Sigma}^{-1}. \tag{3.17}$$

(3) Compute the eigendecomposition of $\tilde{A}$,

$$\tilde{A}W = W\Lambda, \tag{3.18}$$

where columns of W are eigenvectors and Λ is a diagonal matrix containing the corresponding eigenvalues λ_k.

(4) Finally, we can reconstruct the eigendecomposition of A through the decomposition results of $\tilde{A}$. Specifically, the eigenvalues of A and $\tilde{A}$ are equivalent, while the eigenvectors are related by linear transformation. The eigenvectors of A are given by columns of ϕ,

$$\phi = X'\tilde{V}\tilde{\Sigma}^{-1}W. \tag{3.19}$$

In the standard DMD algorithm, the matrix A quantifies the dynamical characteristic between two adjacent snapshots. In the following, a lag τ is introduced into Eq (3.9), i.e., $\boldsymbol{x}_{k+\tau} = A\boldsymbol{x}_k$. Equations (3.10) and (3.11) can be rewritten as,

$$X = \begin{bmatrix} | & | & & | \\ \boldsymbol{x}_1 & \boldsymbol{x}_2 & \cdots & \boldsymbol{x}_{N-\tau} \\ | & | & & | \end{bmatrix}, \tag{3.20}$$

$$\begin{aligned} X' &= \begin{bmatrix} | & | & & | \\ \boldsymbol{x}_{1+\tau} & \boldsymbol{x}_{2+\tau} & \cdots & \boldsymbol{x}_N \\ | & | & & | \end{bmatrix} \\ &= \begin{bmatrix} | & | & & | \\ A\boldsymbol{x}_1 & A\boldsymbol{x}_2 & \cdots & A\boldsymbol{x}_{N-\tau} \\ | & | & & | \end{bmatrix}. \end{aligned} \tag{3.21}$$

In the following, we introduce τ-DMD [22] (as shown in Algorithm 1) to solve the problem of blind chaotic signal separation and blind image separation. It is suitable for low-dimensional matrix attributed to the small number of modes. In order to achieve the unification of BSS and τ-DMD in formula form, the observation matrix is denoted as,

$$\begin{aligned} \boldsymbol{X} &= [X_1(t); X_2(t); \cdots; X_n(t)] \\ &= [\boldsymbol{x}_1, \boldsymbol{x}_2, \cdots, \boldsymbol{x}_N], (t = 1, 2, \cdots, N), \end{aligned} \tag{3.22}$$

where $\boldsymbol{x}_k = [X_1(k); X_2(k); \cdots; X_n(k)], (k = 1, 2, \cdots, N)$.

Step 1: In order to reduce the complexity of τ-DMD, the observed signal $\boldsymbol{X} = [\boldsymbol{x}_1, \boldsymbol{x}_2, \cdots, \boldsymbol{x}_N]$ is centralized so that it is a matrix with zero mean. First of all, subtracting an average $\sigma = \frac{1}{N}\sum_{i=1}^{N} \boldsymbol{x}_i$ from each column of the mixed matrix $\boldsymbol{X} = [\boldsymbol{x}_1, \boldsymbol{x}_2, \cdots, \boldsymbol{x}_N]$, it deduces that,

$$\begin{aligned} \overline{\boldsymbol{X}} &= [\boldsymbol{x}_1 - \sigma, \boldsymbol{x}_2 - \sigma, \boldsymbol{x}_3 - \sigma, \ldots \boldsymbol{x}_N - \sigma] \\ &= [\bar{\boldsymbol{x}}_1, \bar{\boldsymbol{x}}_2, \bar{\boldsymbol{x}}_3, \ldots \bar{\boldsymbol{x}}_N]. \end{aligned} \tag{3.23}$$

Step 2: The τ-DMD algorithm is defined as follows:

$$\overline{\boldsymbol{X}}^{\tau}_{(0)} = [\bar{\boldsymbol{x}}_1, \bar{\boldsymbol{x}}_2, \bar{\boldsymbol{x}}_3, \ldots \bar{\boldsymbol{x}}_{N-\tau}], \tag{3.24}$$

$$\overline{\boldsymbol{X}}^{\tau}_{(1)} = [\bar{\boldsymbol{x}}_{1+\tau}, \bar{\boldsymbol{x}}_{2+\tau}, \bar{\boldsymbol{x}}_{3+\tau}, \ldots \bar{\boldsymbol{x}}_N], \tag{3.25}$$

$$\tilde{A}_{\tau} = \overline{\boldsymbol{X}}^{\tau}_{(1)} \left[\overline{\boldsymbol{X}}^{\tau}_{(0)}\right]^{+}. \tag{3.26}$$

Step 3: The eigendecomposition of $\tilde{A}_{\tau}$ is,

$$\tilde{A}_{\tau} = \tilde{Q} \cdot \tilde{\Lambda} \cdot \tilde{Q}^{-1}, \tag{3.27}$$

where $\tilde{Q}$ is the estimation of the mixed matrix Q, $\tilde{\Lambda}$ is a diagonal matrix for which the eigenvalues are in descending order, and each of the columns in $\tilde{Q}$ are the eigenvector corresponding to the eigenvalue.

Step 4: Based on Eqs (3.2) and (3.23), it can be deduced that,

$$\hat{\boldsymbol{S}} = \tilde{Q}^{-1}\boldsymbol{X}, \tag{3.28}$$

$$\boldsymbol{X} = \overline{\boldsymbol{X}} + \sigma \cdot \mathrm{I}_n^T. \tag{3.29}$$

And then we can get an estimation of the source matrix $\boldsymbol{S}$,

$$\begin{aligned} \hat{\boldsymbol{S}} &= [\hat{S}_1; \hat{S}_2; \cdots; \hat{S}_n] \\ &= \tilde{Q}^{-1}(\overline{\boldsymbol{X}} + \sigma \cdot \mathrm{I}_n^T) = \tilde{Q}^{-1}\overline{\boldsymbol{X}} + \tilde{Q}^{-1} \cdot \sigma \cdot \mathrm{I}_n^T. \end{aligned} \tag{3.30}$$

Algorithm 1. τ-DMD algorithm

Input: The matrix of mixed signals,
$\boldsymbol{X} = [X_1(t); X_2(t); \cdots; X_n(t)] = [\boldsymbol{x}_1, \boldsymbol{x}_2, \cdots, \boldsymbol{x}_N], (t = 1, 2, \cdots, N)$.
1: Substract an average $\sigma = \frac{1}{N}\sum_{i=1}^{N} \boldsymbol{x}_i$ from each column of the mixed matrix $\boldsymbol{X}$, i.e., $\overline{\boldsymbol{X}} = [\boldsymbol{x}_1 - \sigma, \boldsymbol{x}_2 - \sigma, \boldsymbol{x}_3 - \sigma, \ldots \boldsymbol{x}_N - \sigma] = [\bar{\boldsymbol{x}}_1, \bar{\boldsymbol{x}}_2, \bar{\boldsymbol{x}}_3, \ldots \bar{\boldsymbol{x}}_N]$.
2: Arrange the N snapshots into two data matrices,
$\overline{\boldsymbol{X}}^{\tau}_{(0)} = [\bar{\boldsymbol{x}}_1, \bar{\boldsymbol{x}}_2, \bar{\boldsymbol{x}}_3, \ldots \bar{\boldsymbol{x}}_{N-\tau}]$, $\overline{\boldsymbol{X}}^{\tau}_{(1)} = [\bar{\boldsymbol{x}}_{1+\tau}, \bar{\boldsymbol{x}}_{2+\tau}, \bar{\boldsymbol{x}}_{3+\tau}, \ldots \bar{\boldsymbol{x}}_N]$.
Compute $\tilde{A}_\tau = \overline{\boldsymbol{X}}^{\tau}_{(1)} \left[\overline{\boldsymbol{X}}^{\tau}_{(0)}\right]^{+}$.
3: Compute the eigendecomposition of $\tilde{A}_\tau$, i.e., $\tilde{A}_\tau = \tilde{Q} \cdot \tilde{\Lambda} \cdot \tilde{Q}^{-1}$,
where $\tilde{Q}$ is the estimation of the mixed matrix Q.
4: Compute the matrix of separated signals,
$\hat{\boldsymbol{S}} = [\hat{S}_1; \hat{S}_2; \cdots; \hat{S}_n] = \tilde{Q}^{-1}\overline{\boldsymbol{X}} + \tilde{Q}^{-1} \cdot \sigma \cdot \mathrm{I}_n^T$,
where each row is the estimation of the source signal.
Output: Return $\tilde{Q}, \hat{\boldsymbol{S}}$

In this paper, we study the case that the number of source signals equals to the number of observed signals, i.e., $m = n$. For a one-dimensional mixed chaotic signal $X_i(t), (i = 1, 2, \cdots, n; t = 1, 2, \cdots, N)$, it can be regarded as a row of the matrix X in τ-DMD. For a two-dimensional image, the signal should be reconstructed into a one-dimensional vector firstly.

4. Simulations

4.1. Performance criteria

The correlation coefficient [35] between the separated signal and the source signal is used to evaluate the separation performance of the mixed chaotic signals. It is defined as

$$\zeta_{ij} = \zeta(S_i, \hat{S}_j) = \left| \frac{\sum_{t=1}^{N} S_i(t)\hat{S}_j(t)}{\sqrt{\sum_{t=1}^{N} {S_i}^2(t) \sum_{t=1}^{N} \hat{S}_j^2(t)}} \right|, \tag{4.1}$$

where $S_i(t),(i=1,2,\cdots,n;t=1,2,\cdots,N)$ is the source signal, $\hat{S}_j(t),(j=1,2,\cdots,n;t=1,2,\cdots,N)$ is the corresponding separated signal, and N is the length of the time series. The closer the correlation coefficient ζ_{ij} is to 1, the higher similarity between the separated signal and the source signal. SSIM index [36] and PSNR [37] are adopted to evaluate the separation quality of images. SSIM is defined as

$$SSIM(p,q)=\frac{(2\mu_p\mu_q+C_1)(2\sigma_{pq}+C_2)}{(\mu_p{}^2+\mu_q{}^2+C_1)(\sigma_p{}^2+\sigma_q{}^2+C_2)}, \tag{4.2}$$

where μ_p, μ_q are the average values of image p and image q, respectively; and σ_p, σ_q are the variances of image p and q, respectively. σ_{pq} denotes the covariance of p and q. $C_1=(K_1L)^2$ and $C_2=(K_2L)^2$ are two variables to stabilize the division with weak denominator. K_1, $K_2<<1$, L denotes the dynamic range of the pixel-values. In our simulation, $K_1=0.01$, $K_2=0.03$, $L=255$. The SSIM value is between -1 and 1. The closer SSIM index is to 1, the more similar the two images are. PSNR is defined as

$$PSNR=10\times\log_{10}(\frac{255^2}{MSE}), \tag{4.3}$$

where MSE represents the mean square error of the source image and the separated image. In most cases, higher PSNR indicates higher quality of the separation.

4.2. Separation of mixed chaotic signals

1) The separation performance for the mixed signals without noise

In this section, we simulate the separation performance of τ-DMD on a noise-free BSS model, $\boldsymbol{X}=Q*[S_1(t);S_2(t);\cdots;S_n(t)],(t=1,2,\cdots,N)$. The mixed signals are obtained by mixing two source signals generated from Lorenz system. The first source signal $S_1(t),(t=1,2,\cdots,5000)$ is the x phase of Lorenz system with parameters $p_1=\{\sigma=10,\rho=28,\beta=8/3\}$ and initial values $\{x(1)=0.02,y(1)=0.01,z(1)=0.03\}$. The second source signal $S_2(t),(t=1,2,\cdots,5000)$ is the x phase of the Lorenz system with parameters $p_2=\{\sigma=12,\rho=35,\beta=3\}$ and initial values $\{x(1)=0.05,y(1)=0.02,z(1)=0.02\}$. The mixing matrix is selected as $Q=randn(2,2)$. Figure 2(a),(b) shows the source signals S_1-S_2 and the corresponding separated signals $\hat{S}_1$-$\hat{S}_2$ by τ-DMD. We calculate the similarity coefficient $\zeta_{11}=\zeta(S_1,\hat{S}_1)=0.9903$ and $\zeta_{22}=\zeta(S_2,\hat{S}_2)=0.9978$, suggesting that τ-DMD can accurately extract the source signals from the mixed signals.

2) The comparison between τ-DMD and other blind source separation algorithms

In this section, we compare the separation performance of τ-DMD with FastICA [10], JADE [11], Amuse [12], and SOBI [13]. FastICA and JADE algorithms are based on the higher-order statistics (HOS), while Amuse and SOBI are based on second-order statistics (SOS). SOBI and AMUSE works on the whitened data and estimate orthogonal matrices. In contrast to SOBI/AMUSE, τ-DMD works on the data directly and estimates nonorthogonal matrices. We present the separation performance of τ-DMD and the above four algorithms for the observed signals mixed by two source signals S_1, S_2, which are generated from x phase and z phase in Lorenz system with parameters $p=\{\sigma=10,\ \rho=50,\ \beta=8/3\}$ and initial values $\{x(1)=0.02,y(2)=0.01,z(1)=0.03\}$. The mixing matrix is randomly selected as

$$Q=\begin{bmatrix} 1.0061 & 0.2571 \\ -0.6509 & -0.9444 \end{bmatrix}. \tag{4.4}$$

The similarity coefficients $\zeta_{11} = \zeta(S_1, \hat{S}_1)$ and $\zeta_{22} = \zeta(S_2, \hat{S}_2)$ calculated by the above five methods are shown in Figure 3. It suggests that τ-DMD has the best performance in separating the mixed chaotic signals.

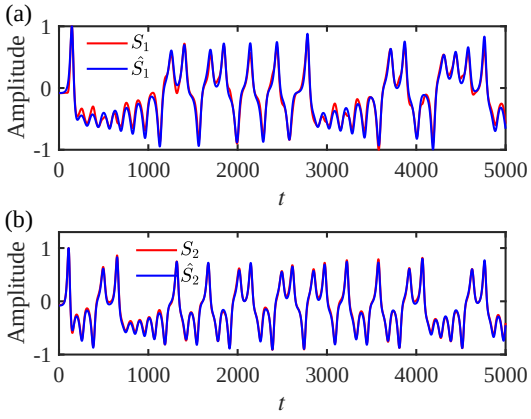

Figure 2. S_1 is the x phase of Lorenz system with parameters $p_1 = \{\sigma = 10, \rho = 28, \beta = 8/3\}$ and initial values $\{x(1) = 0.02, y(1) = 0.01, z(1) = 0.03\}$, S_2 is the x phase of Lorenz system with parameters $p_2 = \{\sigma = 12, \rho = 35, \beta = 3\}$ and initial values $\{x(1) = 0.05, y(1) = 0.02, z(1) = 0.02\}$. (a) The first source signal S_1 (red curve) and the separated signal $\hat{S}_1$ (blue curve) by τ-DMD. (b) The second source signal S_2 (red curve) and the separated signal $\hat{S}_2$ (blue curve) by τ-DMD.

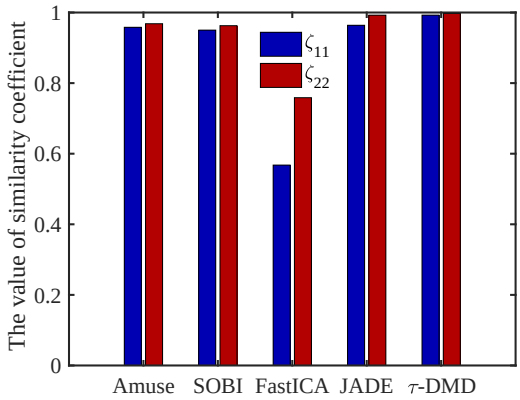

Figure 3. S_1, S_2 are generated from x phase and z phase in Lorenz system, respectively, where the parameters are $p = \{\sigma = 10, \rho = 50, \beta = 8/3\}$ and initial values are $\{x(1) = 0.02, y(2) = 0.01, z(1) = 0.03\}$. The similarity coefficients $\zeta_{11} = \zeta(S_1, \hat{S}_1)$ and $\zeta_{22} = \zeta(S_2, \hat{S}_2)$ are calculated by using Amuse, SOBI, FastICA, JADE, and τ-DMD algorithms.

3) The separation performance for the mixed signals with noise

In this section, we simulate the separation performance of τ-DMD on a BSS model with noise, $\boldsymbol{X} = Q * [S_1(t); S_2(t); \cdots; S_n(t)] + \boldsymbol{n}(t), (t = 1, 2, \cdots, N)$. We add a Gaussian white noise in the mixed

signals. The standard definition of signal-to-noise ratio (*SNR*) [38] is the ratio of signal power to noise power. The formula of *SNR* is defined as:

$$SNR = 10 \times \log_{10}(Ps/Pn), \tag{4.5}$$

where Ps is the signal power and Pn is the noise power. In our simulation, the first source signal $S_1(t), (t = 1,2,\cdots,10000)$ is the y phase of Rossler system with parameters $p = \{a = 0.2, b = 0.4, c = 5.7\}$ and initial values $\{x(1) = 1, y(1) = 0, z(1) = 0\}$ and the second source signal $S_2(t), (t = 1,2,\cdots,10000)$ is the z phase of Lorenz system with parameters $p = \{\sigma = 10, \rho = 50, \beta = 8/3\}$ and initial values $\{x(1) = 0.02, y(1) = 0.01, z(1) = 0.03\}$. The mixing matrix is randomly selected as

$$Q = \begin{bmatrix} 1.4242 & 0.0485 \\ -1.3708 & 1.0426 \end{bmatrix}. \tag{4.6}$$

A Gaussian white noise with *SNR* = 12.3034 dB is added when mixing. Figure 4(a),(b) shows the source signals S_1–S_2 and the corresponding separated signals $\hat{S}_1$–$\hat{S}_2$ by τ-DMD without de-noising. The similarity coefficients are calculated as $\zeta_{11} = 0.9556$ and $\zeta_{22} = 0.6527$. In Figure 4(b), it shows that the second signal cannot be separated accurately due to the high-intensity noise.

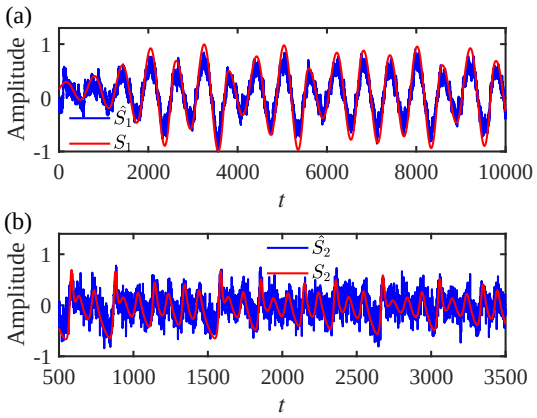

Figure 4. S_1 is the y phase of Rossler system with parameters $p = \{a = 0.2, b = 0.4, c = 5.7\}$ and initial values $\{x(1) = 1, y(1) = 0, z(1) = 0\}$, S_2 is the z phase of Lorenz system with parameters $p = \{\sigma = 10, \rho = 50, \beta = 8/3\}$ and initial values$\{x(1) = 0.02, y(1) = 0.01, z(1) = 0.03\}$. (a) The first source signal S_1 (red curve) and the separated signal $\hat{S}_1$ (blue curve) by τ-DMD without de-noising. (b) The second source signal S_2 (red curve) and the separated signal $\hat{S}_2$ (blue curve) by τ-DMD without de-noising. For a clearer comparison, we present $\{S_2(t), (t = 500, 501, \cdots, 3500)\}$.

In order to accurately separate the second signal S_2 in Figure 4(b), wavelet de-noising [39] based on hard threshold is applied to the matrix $\boldsymbol{X}$ before τ-DMD. Figure 5(a),(b) shows the source signals S_1-S_2 and the corresponding separated signals $\hat{S}_1$-$\hat{S}_2$ by τ-DMD with hard threshold de-noising. The first similarity coefficient ζ_{11} is increased from 0.9556 to 0.9783, and the second similarity coefficient ζ_{22} is from 0.6527 to 0.9193. The results show that the de-noising process improves the quality of

source separation in noisy situations. For the source signals in Figure 4, we calculate the similarity coefficients ζ_{11} and ζ_{22} for different *SNR*, which are shown in Figure 6. The results show that even for low *SNR*, it can still achieve better separation performance by using τ-DMD after hard threshold de-noising.

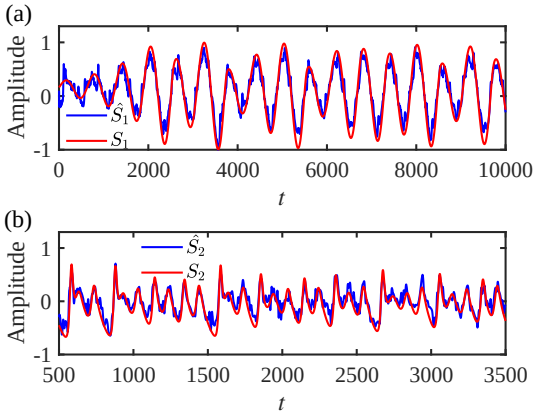

Figure 5. S_1 and S_2 are the source signals in Figure 4, respectively. (a) The first source signal S_1 (red curve) and the separated signal $\hat{S}_1$ (blue curve) by τ-DMD after hard threshold de-noising. (b) The second source signal S_2 (red curve) and the separated signal $\hat{S}_2$ (blue curve) by τ-DMD after hard threshold de-noising. For a clearer comparison, we present $\{S_2(t), (t = 500, 501, \cdots, 3500)\}$.

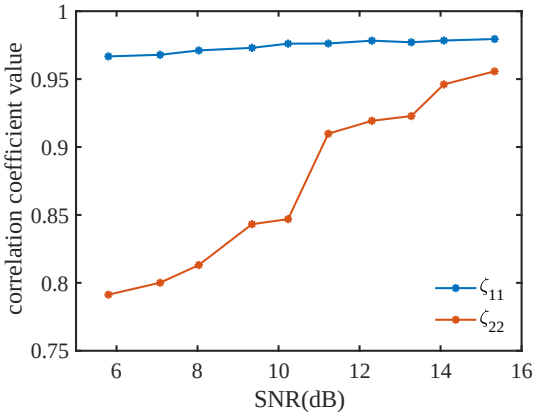

Figure 6. S_1 and S_2 are the source signals in Figure 4. The abscissa is the *SNR*. The ordinate is the correlation coefficient $\zeta_{11} = \zeta(S_1, \hat{S}_1)$ and $\zeta_{22} = \zeta(S_2, \hat{S}_2)$ calculated by τ-DMD after hard threshold de-noising under different *SNR*.

4) Application: A semi-simulated study of noise removal from electrocardiogram (ECG) and artifact removal from electroencephalogram (EEG) based on τ-DMD

EEG and ECG are non-invasive imaging methods that can be used to measure different brain and heart states, with the advantages of portability, low cost, and high temporal resolution. However, EEG and ECG signals are often contaminated with noise and artifacts (such as ocular and muscle artifacts),

which make the data analysis of EEG and ECG more difficult. Although some other methods [40, 41] have been used to remove noise and artifacts in ECG and EEG, so far no literature has been reported using τ-DMD on the study of these problems.

In this section, we present the semi-simulation of applying τ-DMD to remove the non-physiological noise from ECG and the ocular artifacts from EEG based on two-channel mixed signals. In the simulation of ECG, Gaussian white noise with zero mean and unit variance is chosen as the non-physiological noise, and the pure ECG source is selected from the first ECG file of the MIT-BIH arrhythmia database [42]; the largest Lyapunov exponent of ECG is calculated to be $0.0188 > 0$, which suggests the ECG signal is chaotic. The mixing matrix is randomly selected as follows,

$$Q = \begin{bmatrix} 0.90 & 0.05 \\ 0.80 & 0.10 \end{bmatrix}. \tag{4.7}$$

The original ECG signal S_1 and the original noise signal S_2 are shown in Figure 7(a),(b). The mixed signals are shown in Figure 7(c),(d). The separated signals $\hat{S}_1$ and $\hat{S}_2$ along with their original signals are shown in Figure 7(e),(f). It shows that τ-DMD can separate the ECG signal and noise well from the mixed signals.

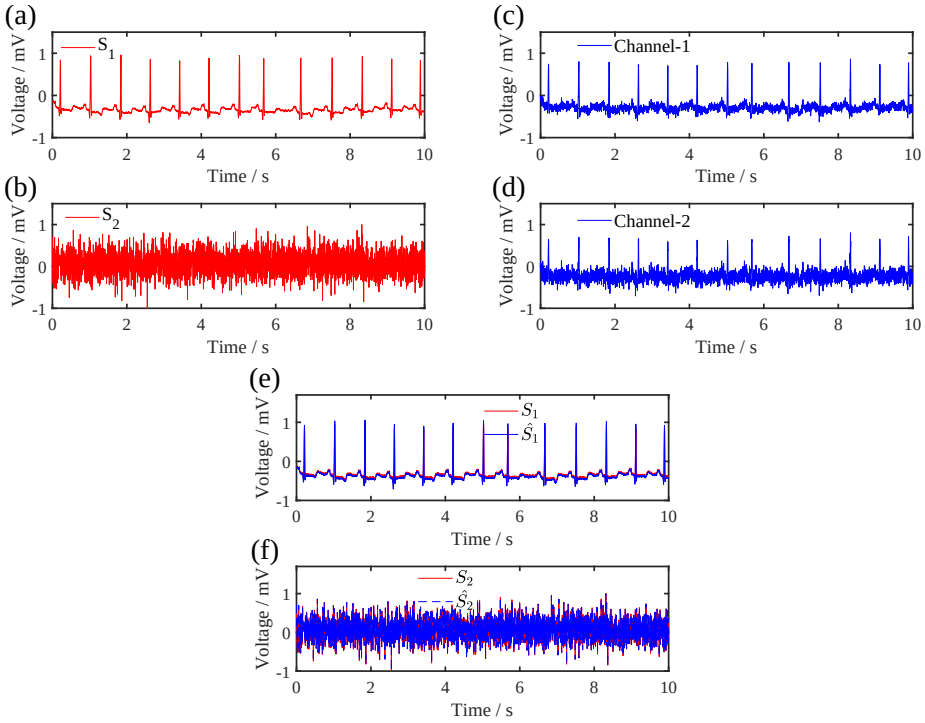

Figure 7. Semi-simulation of ECG using τ-DMD. (a),(b) A 10 s pure ECG signal and a 10 s pure noise signal. (c),(d) Mixture of ECG and noise signals with two channels. (e),(f) Separation of the noise signal and the original ECG signal.

In the semi-simulation of EEG, we remove ocular artifacts from the EEG by using τ-DMD. The pure ocular artifacts source signal is obtained by processing the data sub093 through Letswave7 [https://letswave.cn/]. The ocular artifacts consist of a wink artifact and a lateral eye movement

artifact. The mixing matrix is randomly selected as follows,

$$Q = \begin{bmatrix} 0.9 & 0.6 \\ 0.8 & 0.8 \end{bmatrix}. \tag{4.8}$$

The original EEG signal S_1 and the ocular artifacts signal S_2 are shown in Figure 8(a),(b). The largest Lyapunov exponents of S_1 and S_2 are calculated as 0.0046 and 0.0066, respectively. It indicates that the source signals S_1 and S_2 in our simulation are chaotic. The mixed signals are shown in Figure 8(c),(d). The separated signals $\hat{S}_1$ and $\hat{S}_2$ along with their original signals are shown in Figure 8(e),(f), suggesting that τ-DMD can separate the EEG signal and ocular artifacts well from the mixed signals.

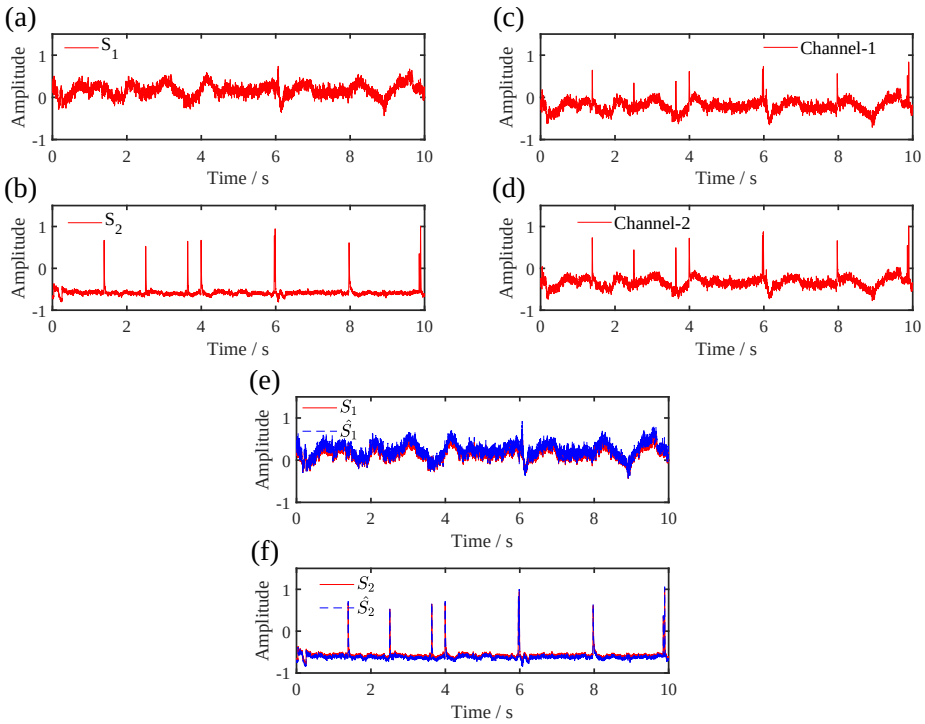

Figure 8. Semi-simulation of EEG using τ-DMD. (a),(b) Original EEG source and ocular artifacts source. (c),(d) Mixture of source signals with two channels. (e),(f) Separation of two source signals.

4.3. Separation of mixed images

Image aliasing is caused by various reasons in the process of image acquisition and transmission. In this section, we study the separation performance of τ-DMD in natural pictures, texture pictures, and text pictures.

1) We separate the linear mixtures of two standard images Lena and Baboon (see Figure 9(a)). Both images are grayscale images with 256×256 pixels, and the two mixing images (see Figure 9(b)) are obtained by the mixing matrix

$$Q = \begin{bmatrix} 0.6 & 0.4 \\ 0.4 & 0.6 \end{bmatrix}. \tag{4.9}$$

According to Figure 9(c)–(e), it shows that the separation by using τ-DMD is better than JADE [11] and ICA based on Kurtosis [43]. Tables 1 and 2 show the comparison between τ-DMD, JADE, and ICA with SSIM and PSNR.

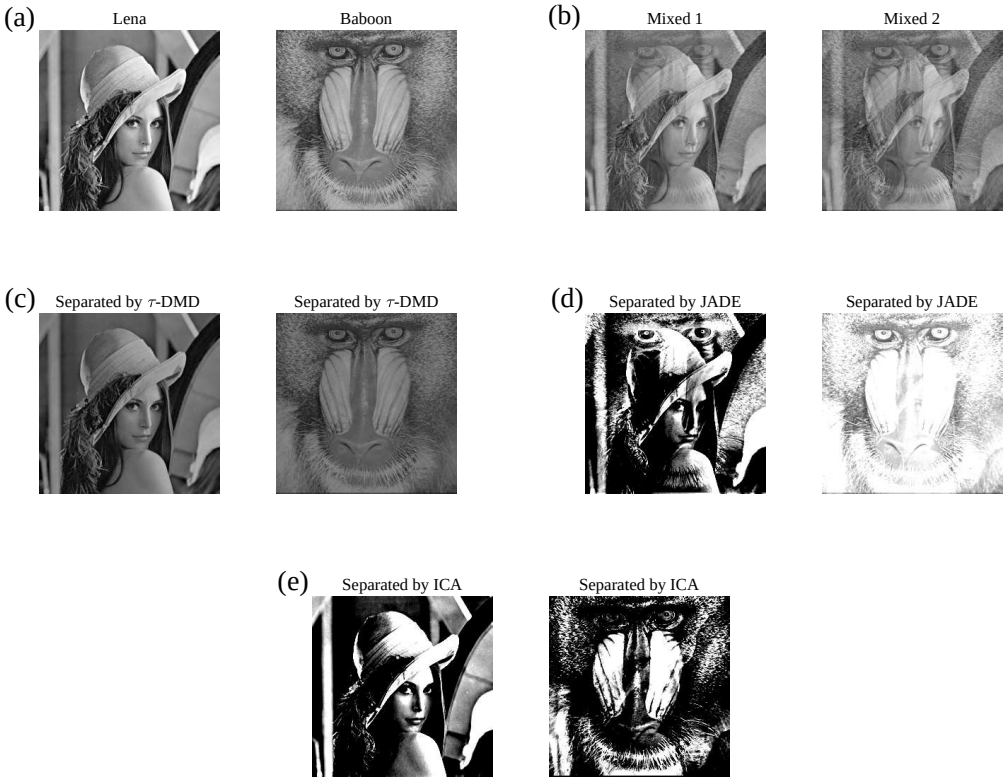

Figure 9. (a) The original images. (b) The linear mixed images. (c) The separated results by τ-DMD. (d) The separated results by JADE. (e) The separated results by ICA.

2) For the old pictures, the images are not clear due to the influence of several types of degradation. The most common situation is that the pictures are both degraded and contaminated by different levels of noise. In this part, we use Gaussian white noise with unit variance to simulate external noise and separate the original images from the mixed images by τ-DMD. The original image and the Gaussian white noise are shown in Figure 10(a). The mixed images are shown in Figure 10(b). It shows that τ-DMD can separate the original images accurately (see Figure 10(c)).

Table 1. The comparison of SSIM by using τ-DMD, JADE, and ICA for Lena and Baboon.

Methods	Lena	Baboon
τ-DMD	0.9966	0.9973
JADE	0.9133	0.9701
ICA	0.9063	0.8928

Table 2. The comparison of PSNR by using τ-DMD, JADE, and ICA for Lena and Baboon.

Methods	Lena	Baboon
τ-DMD	64.1947	65.3408
JADE	49.0775	54.3760
ICA	48.8731	47.8009

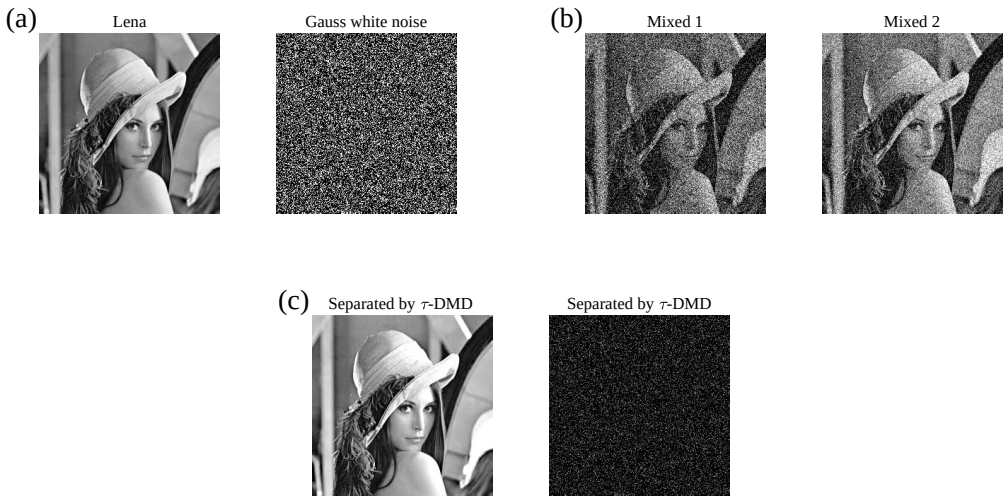

Figure 10. (a) The original image and Gaussian white noise. (b)The linear mixed images. (c) The separated results by τ-DMD.

3) We separate the mixed fingerprint images, which is of great significance to criminal investigation. Two different fingerprint images are shown in Figure 11(a), and the mixed images (see Figure 11(b)) are linearly aliased by the matrix

$$Q = \begin{bmatrix} 0.2511 & 0.4416 \\ 0.3909 & 0.1670 \end{bmatrix}. \tag{4.10}$$

The separated fingerprint images by τ-DMD, JADE, and ICA are shown in Figure 11(c)–(e). Tables 3 and 4 show the comparison between τ-DMD, JADE, and ICA with SSIM and PSNR. It shows that the separation by using τ-DMD is better than JADE and ICA.

4) We separate two overlapped text images (see Figure 12(a),(b)) with show-through because the paper is not completely opaque [44]. The clean overwriting and underwriting texts are separated by using τ-DMD. We compare the separation results based on τ-DMD(See Figure 12(c),(d)) and JADE (see Figure 12(e),(f)). Clearly, τ-DMD does a better job in separating the real-life text images than JADE. In this paper, we introduce a new method, τ-DMD, to separate the overlapped text images, and it shows a good separation result, which is conducive to the text recognition.

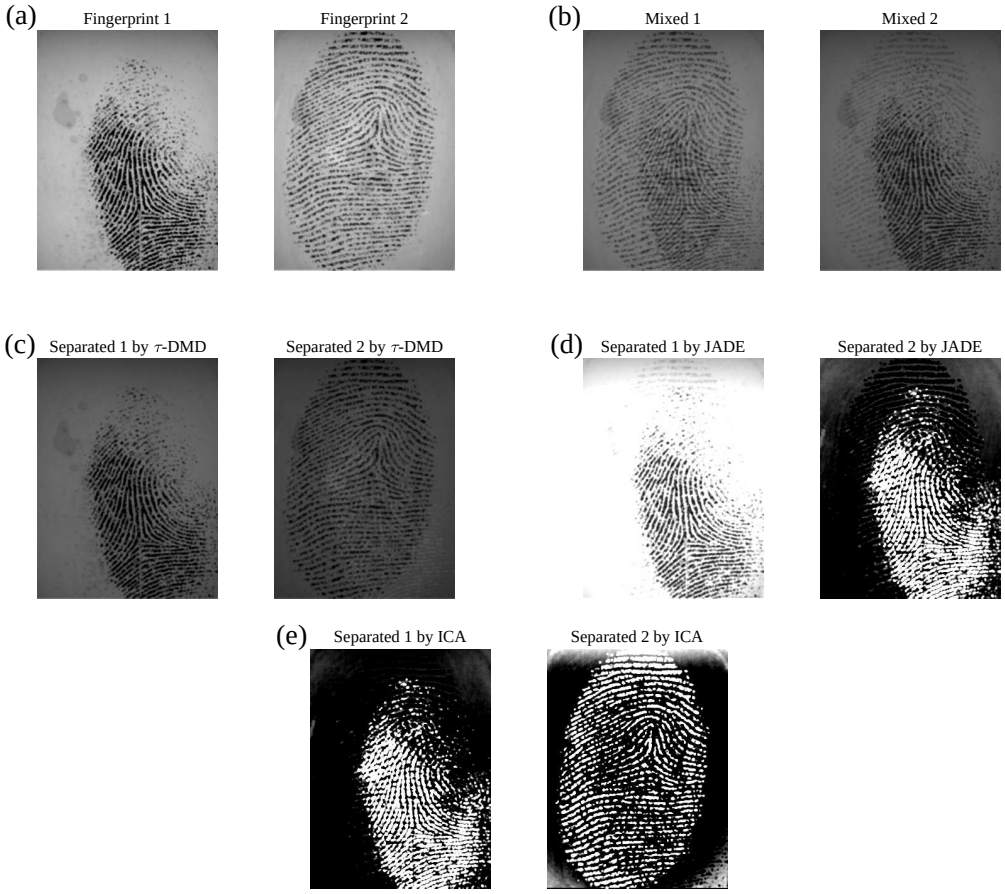

Figure 11. (a) The original images. (b) The linear mixed images. (c) The separated results by τ-DMD. (d) The separated results by JADE. (e) The separated results by ICA.

Table 3. The comparison of SSIM by using τ-DMD, JADE, and ICA for Fingerprint 1 and Fingerprint 2.

Methods	Fingerprint 1	Fingerprint 2
τ-DMD	0.9897	0.9801
JADE	0.9791	0.9008
ICA	0.8584	0.8439

Table 4. The comparison of PSNR by using τ-DMD, JADE, and ICA for Fingerprint 1 and Fingerprint 2.

Methods	Fingerprint 1	Fingerprint 2
τ-DMD	59.4206	56.6565
JADE	55.8735	47.9623
ICA	45.5921	45.7191

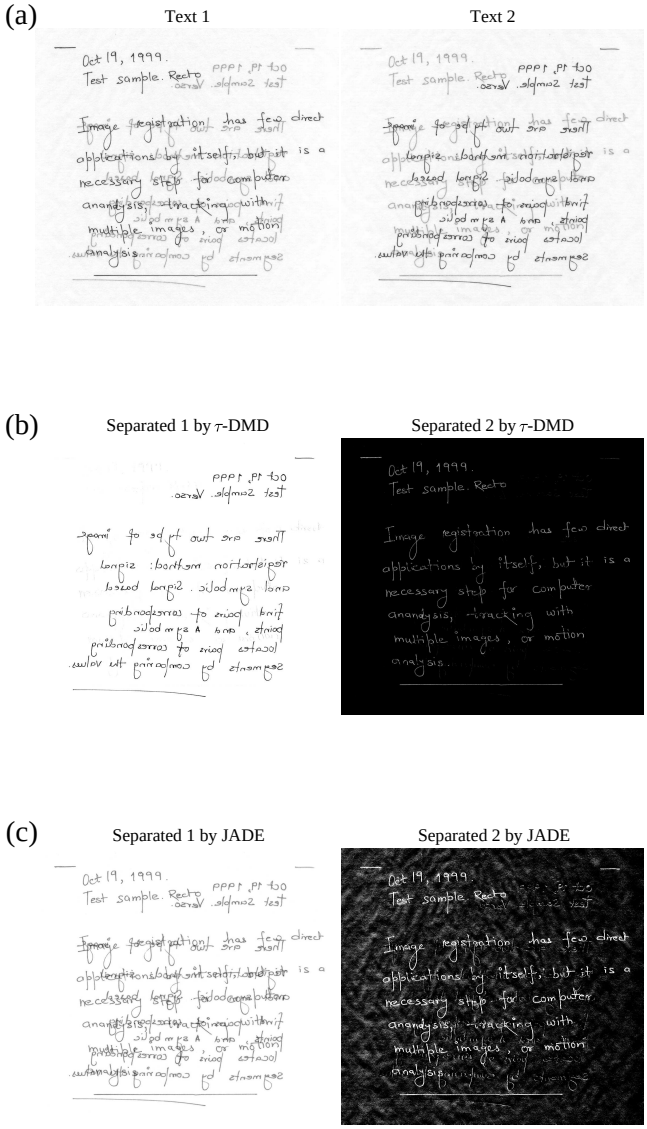

Figure 12. (a) The real-life text images. (b) The separated results by τ-DMD. (c) The separated results by JADE.

5) Application: images encryption and decryption

The block diagram of the BSS-based images encryption [45] and decryption is shown in Figure 13. $S_1(t), S_2(t), ...S_n(t)(t = 1,2,...N)$ are a group of original images to be encrypted simultaneously, where N is the size (data length) of each image. $K_1(t), K_2(t), ...K_n(t), (t = 1,2,...N)$ are n key images for encrypting the original images. I_0 is the secret seed of the pseudorandom number generator (PRNG) in the key images generating algorithm. In this paper, the Chen chaotic system is chosen as a pseudorandom sequence generator, which has good pseudorandom characteristics [46]. The Chen system is only used as an example of a pseudorandom values generator, and researchers should design

a more secure PRNG generation algorithm if a higher level of security is required.

The encryption equation is as follows,

$$\boldsymbol{X}(t) = Q\boldsymbol{S}_{new}(t), \tag{4.11}$$

where $\boldsymbol{S}_{new}(t) = [S_1(t); S_2(t); ...S_n(t); K_1(t); K_2(t); ...K_n(t)]$, Q is a $n \times 2n$ underdetermined mixing matrix.

On the receiving side, once the encrypted images $X_1(t), X_2(t), ...X_n(t)$ are received and the n key images $K_1(t), K_2(t), ...K_n(t)$ are regenerated with the secret seed I_0 provided, they are combined to form $2n$ mixed signals $\boldsymbol{X}_{new} = [X_1(t); X_2(t); ...X_n(t); K_1(t); K_2(t); ...K_n(t)]$. Construct

$$\boldsymbol{X}_{new} = Q_{new}\boldsymbol{S}_{new}, \tag{4.12}$$

where $Q_{new} = \begin{bmatrix} Q(1:n) & Q(n+1:2n) \\ \mathbf{0} & \boldsymbol{I} \end{bmatrix}$, $Q(1:n)$ is the first n columns of the underdetermined mixing matrix Q and $Q(n+1:2n)$ corresponds to the last n columns; $\mathbf{0}$ is a $n \times n$ zero matrix and $\boldsymbol{I}$ is a $n \times n$ identity matrix. Obviously, Q_{new} is a $2n \times 2n$ square matrix of full rank. Accordingly, with the key images regenerated, the underdetermined BSS problem resulting from the encryption becomes the conventional BSS, so that the original images can be well recovered through τ-DMD.

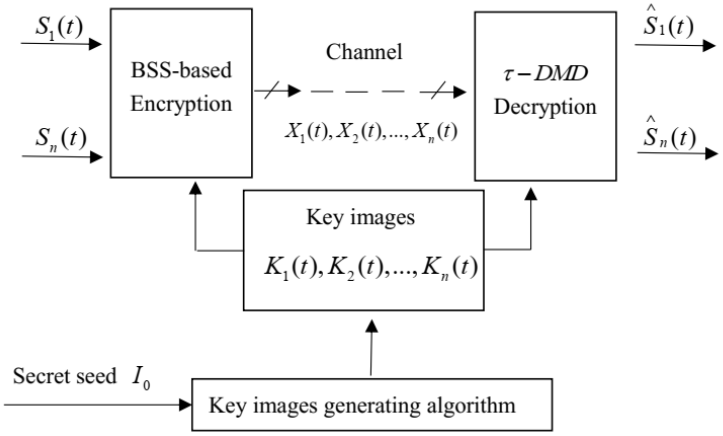

Figure 13. BSS-based image encryption.

We also need to explain that it is impossible to separate the original images without the key images. In the encryption process, construct the underdetermined mixing matrix Q as,

$$Q = \begin{bmatrix} BC & B \end{bmatrix}, \tag{4.13}$$

where B and C are two $n \times n$ matrixes of full rank [45]. To achieve the security goal, the original images must be covered by the key images with much higher level of energy. The values of matrix element in B must be larger than those in BC. Acorrding to Eqs (4.11) and (4.13),

$$\begin{aligned} \boldsymbol{X} = \begin{bmatrix} BC & B \end{bmatrix} [S_1(t); ...; S_n(t); K_1(t); ...; K_n(t)] \\ = BC * \boldsymbol{S}(t) + B * \boldsymbol{K}(t), \end{aligned} \tag{4.14}$$

Combined with Eq (3.3), it can be deduced that

$$\boldsymbol{Y}(t) = W\boldsymbol{X}(t) = WBC\boldsymbol{S}(t) + WB\boldsymbol{K}(t). \tag{4.15}$$

Considering the key images $\boldsymbol{K}(t)$ are the main component in the encrypted images, i.e., $WB = PD$. Finally, we get the separated signals

$$\boldsymbol{Y}(t) = PD\left[C\boldsymbol{S}(t) + \boldsymbol{K}(t)\right]. \tag{4.16}$$

It means that the BSS output signals are covered by the key images, which can achieve image security without the key images.

In the first experiment, the original image Lena of size 256×256 and the key image generated by Chen chaotic system with seed $\mathrm{I}_0 = \{(a = 35, b = 3, c = 28); (x_0 = -3, y_0 = 2, z_0 = 20)\}$ are shown in Figure 14(a). The encrypted image obtained by the underdetermined mixing matrix $Q = \begin{bmatrix} 0.2 & 0.8 \end{bmatrix}$ is shown in Figure 14(b); the original image can be well masked by the key image in the encrypted image. Comparing the decryption results by τ-DMD and FastICA (see Figure 14(c),(d)), it shows that τ-DMD can extract the source image more accurately. In the second experiment, two natural images, Lena and Baboon, are shown in Figure 15(a); two key images $K_1(t), K_2(t)$ (see Figure 15(b)) are generated by Chen chaotic system with seed $\mathrm{I}_0 = \{(a = 30, b = 4, c = 29); (x_0 = -1, y_0 = 5, z_0 = 10)\}$ and seed $\mathrm{I}_0 = \{(a = 35, b = 3, c = 28); (x_0 = -3, y_0 = 2, z_0 = 20)\}$, respectively. The encrypted images obtained by the underdetermined mixing matrix

$$Q = \begin{bmatrix} 0.2 & 0.3 & 0.8 & 0.9 \\ 0.15 & 0.25 & 0.7 & 0.8 \end{bmatrix}, \tag{4.17}$$

are shown in Figure 15(c); Figure 15(d) shows the encrypted images by τ-DMD.

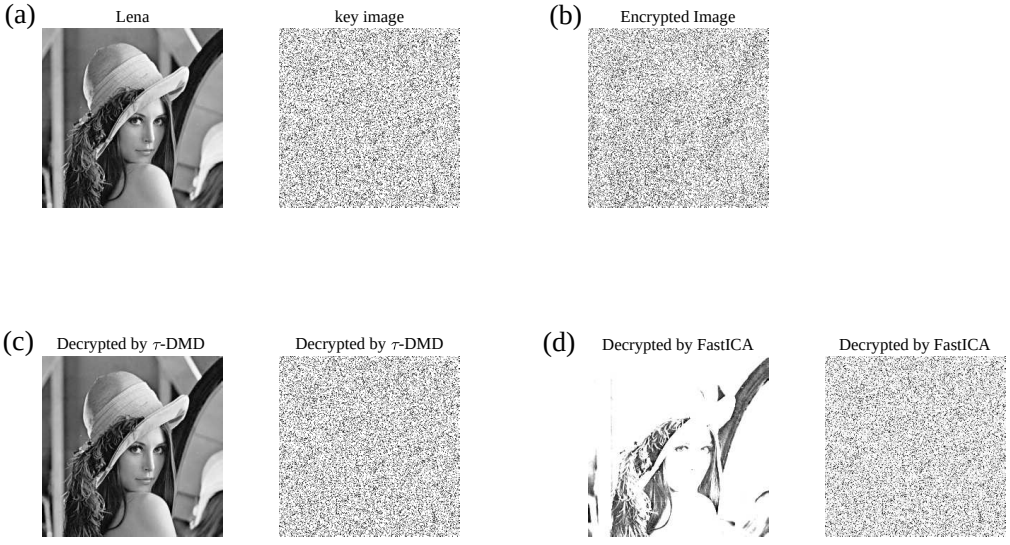

Figure 14. (a) Original image Lena and image. (b) The encrypted image. (c) The decrypted image by τ-DMD. (d) The decrypted image by FastICA.

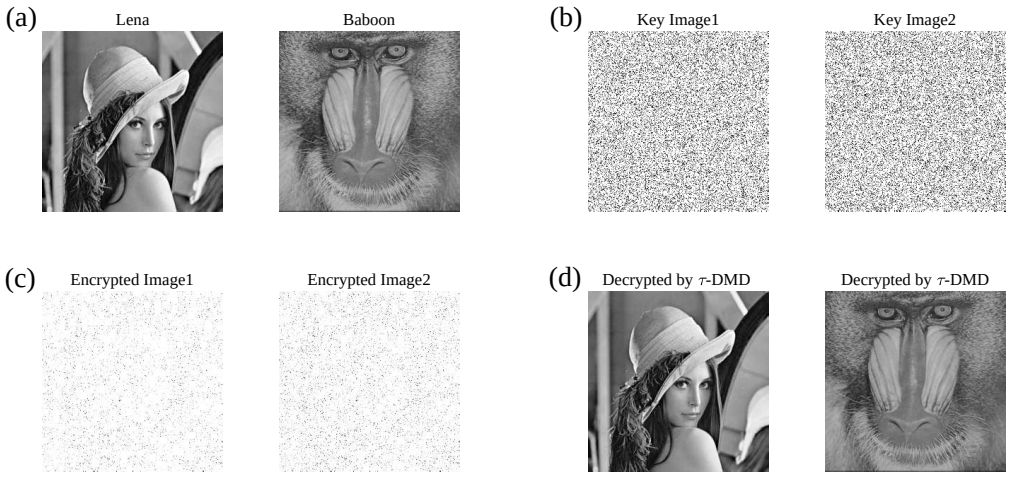

Figure 15. (a) Two original images Lena and Baboon. (b) Two key images. (c) Two encrypted images. (d) Two decrypted images by τ-DMD.

5. Conclusions

In this paper, we introduce a novel approach τ-DMD to solve the separation of mixed chaotic signals and mixed images. τ-DMD fully utilizes the principle of decomposing the observed mixed signals to a set of non-orthogonal modes that represent the evolution of the source signals.

Two cases are taken into consideration in the separation of chaotic signals: namely, the mixture is noiseless or contaminated by noise. For the first case, we verify the separation performance of τ-DMD on the chaotic signals generated by Lorenz system. Comparing with the existing classical blind source separation algorithms (Amuse, SOBI, FastICA and JADE), τ-DMD shows a better separation performance. For the second case, wavelet threshold de-noising is used in the preprocessing of the mixed signals, and then τ-DMD is used to the denoised mixed signals, showing a better separability under high intensity noise. In the application, we use τ-DMD to eliminate the hidden noise from two-channel ECG signals, and remove the ocular artifacts from two-channel EEG signals. τ-DMD can provide a new way of processing the measured medical data.

For the image-mixture blind source separation problem, τ-DMD can accurately separate the linear mixed images. Three test cases are used, including a set of two different natural photographs, a set of two similar fingerprint images, and a set of two different text images. It suggests that there is improvement in separability for τ-DMD compared with other algorithms. For instance, when comparing τ-DMD to JADE on the real-life text images, we see that τ-DMD provides clearer separation results. For the application in images, τ-DMD is used to extract the original images in the process of decryption with the secret seeds provided. Two simulations are performed to illustrate the performance of τ-DMD for image decryption, and it demonstrates that τ-DMD can achieve a higher level of decryption quality from the encrypted images than FastICA.

τ-DMD may find its application in multi-user chaotic communication systems and wireless sensor networks. It can be discussed from the following aspects: (1) In a multi-user chaotic communications scheme, several users share a common channel. Each user's information is modulated with a different

chaotic system and the information is transmitted independently. However, the receiver gets a mixture of each user's signal and additional noise. The goal is to extract the chaotic signal sent by each user and then the message information can be acquired. (2) In wireless sensor networks, the signals received by the terminal processor are usually complex mixed chaotic signals. The engineering needs to separate the useful signal from the mixed signal to perform the next transmission analysis, and τ-DMD can provide a new way of solving this problem.

τ-DMD can be applied to astrophysical images and document images processing. It can be discussed from the following aspects: (1) Astrophysical radiation images contain various cosmological components such as the cosmic microwave background radiation, galactic dust, synchrotron, and extragalactic radio sources. We can extract individual components from multiple astrophysical images by using τ-DMD. All these components carry important information, and they are of great importance to the research in astronomy. (2) Documents (such as foot prints collected at the scene, printed books, and photos) are often affected by several types of degradation. In some cases, it can be seen as a mixture of various components and external noise, and effective separation by τ-DMD can facilitate the storage and utilization of these documents. Furthermore, τ-DMD could be applied in stock prediction or infectious disease prediction. The video processing based on the separation of foreground and background can be achieved by τ-DMD, which can be applied in environmental monitoring.

Use of AI tools declaration

The authors declare they have not used Artificial Intelligence (AI) tools in the creation of this article.

Acknowledgments

This work was supported by the NSFC grant (No. 52071298).

Conflict of interest

The views expressed in this article are not necessarily those of the banks the author works with. Please direct any comments to the author Cun Chen at: chencun@zzu.edu.cn.

References

1. Koopman BO, (1931) Hamiltonian systems and transformation in Hilbert space. *Proc Nat Acad Sci* 17: 315-318. https://doi.org/10.1073/pnas.17.5.315
2. Schmid PJ, (2010) Dynamic mode decomposition of numerical and experimental data. *J Fluid Mech* 656: 5-28. https://doi.org/10.1017/S0022112010001217
3. Rowley CW, Mezić I, Bagheri S, Schlatter P, Henningson DS, (2009) Spectral analysis of nonlinear flows. *J Fluid Mech* 641: 115-127. https://doi.org/10.1017/S0022112009992059
4. Abdi H, Williams LJ, (2010) Principal component analysis. *Wiley Interdiscip Rev Comput Stat* 2: 433-459. https://doi.org/10.1002/wics.101

5. Chen KK, Tu JH, Rowley CW, (2012) Variants of dynamic mode decomposition: Boundary condition, Koopman, and Fourier analyses. *J Nonlinear Sci* 22: 887-915. https://doi.org/10.1007/s00332-012-9130-9

6. Brunton SL, Kutz JN, (2019) *Data-Driven Science and Engineering,* Cambridge: Cambridge Univ. Press. https://doi.org/10.1017/9781108380690

7. Yost WA, (1997) The cocktail party problem: Forty years later, In: *Binaural and Spatial Hearing in Real and Virtual Environments,* Mahwah, NJ, USA: Lawrence Erlbaum, 329-347.

8. Visser E, Lee TW, (2003) Application of blind source separation in speech processing for combined interference removal and robust speaker detection using a two-microphone setup, In: *Proc. of ICA2003,* 325-329.

9. Rieta JJ, Castells F, Snchez C, Zarzoso V, Millet J, (2004) Atrial activity extraction for atrial fibrillation analysis using blind source separation. *IEEE Trans Biomed Eng* 51: 1176-1186. https://doi.org/10.1109/TBME.2004.827272

10. Comon P, Jutten C, (2010) *Handbook of Blind Source Separation: Independent Component Analysis and Applications,* Oxford, U.K.: Academic.

11. Miettinen J, Nordhausen K, Taskinen S, (2017) Blind source separation based on joint diagonalization in R: The packages JADE and BSSasymp. *J Stat Softw* 76: 1-31. https://doi.org/10.18637/jss.v076.i02

12. Tong L, Soon VC, Huang YF, Liu R, (1990) AMUSE: A new blind identification algorithm, In: *IEEE International Symposium on Circuits and Systems*, 1784-1787. https://doi.org/10.1109/ISCAS.1990.111981

13. Belouchrani A, Abed-Meraim K, Cardoso JF, Moulines E, (1997) A blind source separation technique using second-order statistics. *IEEE Trans Signal Process* 45: 434-444. https://doi.org/10.1109/78.554307

14. Proctor JL, Eckhoff PA, (2015) Discovering dynamic patterns from infectious disease data using dynamic mode decomposition. *Int Health* 7: 139-145. https://doi.org/10.1093/inthealth/ihv009

15. Brunton BW, Johnson LA, JG Ojemann, JN Kutz, (2016) Extracting spatial-temporal coherent patterns in large-scale neural recordings using dynamic mode decomposition. *J Neurosci Meth* 258: 1-15. https://doi.org/10.1016/j.jneumeth.2015.10.010

16. Berger E, Sastuba M, Vogt D, Jung B, Ben Amor H, (2015) Estimation of perturbations in robotic behavior using dynamic mode decomposition. *Adv Robotics* 29: 331-343. https://doi.org/10.1080/01691864.2014.981292

17. Grosek J, Kutz JN, (2014) Dynamic mode decomposition for realtime background/foreground separation in video. preprint, arXiv: 1404.7592. https://doi.org/10.48550/arXiv.1404.7592

18. Mann J. Kutz JN, (2016) Dynamic mode decomposition for financial trading strategies. *Quant Finance* 16: 1643-1655. https://doi.org/10.1080/14697688.2016.1170194

19. Barocio E, Pal BC, Thornhill NF, Messina AR, (2015) A dynamicmode decomposition framework for global power system oscillation analysis. *IEEE Trans Power Syst* 30: 2902-2912. https://doi.org/10.1109/TPWRS.2014.2368078

20. Kutz JN, Fu X, Brunton SL, (2016) Multiresolution dynamic mode decomposition. *SIAM J Appl Dyn Syst* 15: 713-735. https://doi.org/10.1137/15M1023543

21. Bai Z, Kaiser E, Proctor JL, Kutz JN, Brunton SL, (2020) Dynamic mode decomposition for compressive system identification. *AIAA J* 58: 561-574. https://doi.org/10.2514/1.J057870

22. Prasadan A, Nadakuditi RR, (2020) Time series source separation using dynamic mode decomposition. *SIAM J Appl Dyn Syst* 19: 1160-1199. https://doi.org/10.1137/19M1273256

23. Arena P, Buscarino A, Fortuna L, Frasca M, (2006) Separation and synchronization of piecewise linear chaotic systems. *Phys Rev E* 74: 026212. https://doi.org/10.1103/PhysRevE.74.026212

24. Xie ZB, Feng JC, (2010) Blind source separation of continuous-time chaotic signals based on fast random search algorithm. *IEEE Trans Circuits II* 57: 461-465. https://doi.org/10.1109/TCSII.2010.2047325

25. Lo T, Leung H, Litva J, (1996) Separation of a mixture of chaotic signals, In: *1996 IEEE International Conference on Acoustics, Speech, and Signal Processing Conference Proceedings* 3: 1798-1801. https://doi.org/10.1109/ICASSP.1996.544216

26. Kuraya M, Uchida A, Yoshimori S, Umeno K, (2008) Blind source separation of chaotic laser signals by independent component analysis. *Opt Express* 16: 725-730. https://doi.org/10.1364/OE.16.000725

27. Lü SX, Wang ZS, Hu ZH, Feng JC, (2014) Gradient method for blind chaotic signal separation based on proliferation exponent. *Chin Phys B* 23: 010506. https://doi.org/10.1088/1674-1056/23/1/010506

28. Krishnagopal S, Girvan M, Ott E, Hunt BR, (2020) Separation of chaotic signals by reservoir computing. *Chaos* 30. https://doi.org/10.1063/1.5132766

29. Guidara R, Hosseini S, Deville Y, (2009) Maximum likelihood blind image separation using nonsymmetrical half-plane markov random fields, *IEEE Trans Image Process* 18: 2435-2450. https://doi.org/10.1109/TIP.2009.2027367

30. Chen N, De Leon P, (2001) Blind image separation through kurtosis maximization, In: *Conference Record of Thirty-Fifth Asilomar Conference on Signals, Systems and Computers (Cat. No. 01CH37256)* 1: 318-322. https://doi.org/10.1109/ACSSC.2001.986936

31. Hara K, Inoue K, Urahama K, (2013) Generalized mixture ratio based blind image separation. *IEEE Signal Proc Lett* 20: 743-746. https://doi.org/10.1109/LSP.2013.2265274

32. Abolghasemi V, Ferdowsi S, Sanei S, (2012) Blind separation of image sources via adaptive dictionary learning. *IEEE Trans Image Process* 21: 2921-2930. https://doi.org/10.1109/TIP.2012.2187530

33. Guo L, Garland M, (2006) The use of entropy minimization for the solution of blind source separation problems in image anslysis. *Pattern Recogn* 39: 1066-1073. https://doi.org/10.1016/j.patcog.2005.09.006

34. Kutz JN, Brunton SL, Brunton BW, Proctor JL, (2016) D*ynamic Mode Decomposition: Data-Driven Modeling of Complex Systems*, Society for Industrial and Applied Mathematics. https://doi.org/10.1137/1.9781611974508

35. Farina D, Févotte C, Doncarli C, Merletti R, (2004) Blind separation of linear instantaneous mixtures of nonstationary surface myoelectric signals. *IEEE Trans Biomed Eng* 51: 1555-1567. https://doi.org/10.1109/TBME.2004.828048
36. Wang Z, Bovik AC, Sheikh HR, Simoncelli EP, (2004) Image quality assessment: From error visibility to structural similarity. *IEEE Trans Image Process* 13: 600-612. https://doi.org/10.1109/TIP.2003.819861
37. Dong W, Zhang L, Lukac R, Shi G, (2013) Sparse representation based image interpolation with nonlocal autoregressive modeling. *IEEE Trans Image Process* 22: 1382-1394. https://doi.org/10.1109/TIP.2012.2231086
38. Säckinger E, (2005) *Broadband Circuits for Optical Fiber Communication*, John Wiley & Sons. https://doi.org/10.1002/0471726400
39. Min QI, Huang S, (2012) Research on Wavelet threshold denoising method based on MATLAB. *Chin J Electron Dev* 35: 103-106.
40. Chawla MPS, Verma HK, Kumar V, (2008) Artifacts and noise removal in electrocardiograms using independent component analysis. *Int J Cardiol*, 129: 278-281. https://doi.org/10.1016/j.ijcard.2007.06.037
41. Wang G, Teng C, Li K, Zhang Z, Yan X, (2016) The removal of EOG artifacts from EEG signals using independent component analysis and multivariate empirical mode decomposition. *IEEE J Biomed Health Inf* 20: 1301-1308. https://doi.org/10.1109/JBHI.2015.2450196
42. PhysioNet, Records in the MIT-BIH arrhythmia database. Available from: https://physionet.org/physiobank/database/html/mitdbdir/records.htm
43. Roweis S, Kurtosis Maximization ICA, 2010. Available from: https://cs.nyu.edu/∼roweis/kica.html
44. Tonazzini A, Gerace I, Martinelli F, (2010) Multichannel blind separation and deconvolution of images for document analysis. *IEEE Trans Image Process* 19: 912-925. https://doi.org/10.1109/TIP.2009.2038814
45. Lin QH, Yin FL, Mei TM, Liang H, (2008) A blind source separation-based method for multiple images encryption. *Image Vis Comput* 26: 788-798. https://doi.org/10.1016/j.imavis.2007.08.017
46. Hu H, Liu L, Ding ND, (2013) Pseudorandom sequence generator based on the chen chaotic system. *Comput Phys Commun* 184: 765-768. https://doi.org/10.1016/j.cpc.2012.11.017

AIMS Press